LOD Generation for Urban Scenes

YANNICK VERDIE, FLORENT LAFARGE and PIERRE ALLIEZ
INRIA Sophia Antipolis

We introduce a novel approach that reconstructs 3D urban scenes in the form of levels of detail (LODs). Starting from raw data sets such as surface meshes generated by multi-view stereo systems, our algorithm proceeds in three main steps: classification, abstraction and reconstruction. From geometric attributes and a set of semantic rules combined with a Markov random field, we classify the scene into four meaningful classes. The abstraction step detects and regularizes planar structures on buildings, fits icons on trees, roofs and facades, and performs filtering and simplification for LOD generation. The abstracted data are then provided as input to the reconstruction step which generates watertight buildings through a min-cut formulation on a set of 3D arrangements. Our experiments on complex buildings and large scale urban scenes show that our approach generates meaningful LODs while being robust and scalable. By combining semantic segmentation and abstraction it also outperforms general mesh approximation approaches at preserving urban structures.

Categories and Subject Descriptors: I.3.5 [**Computer Graphics**]: Computational Geometry and Object Modeling

Additional Key Words and Phrases: urban reconstruction, levels of detail, abstraction, iconization, Markov random field, min-cut formulation, arrangement of planes.

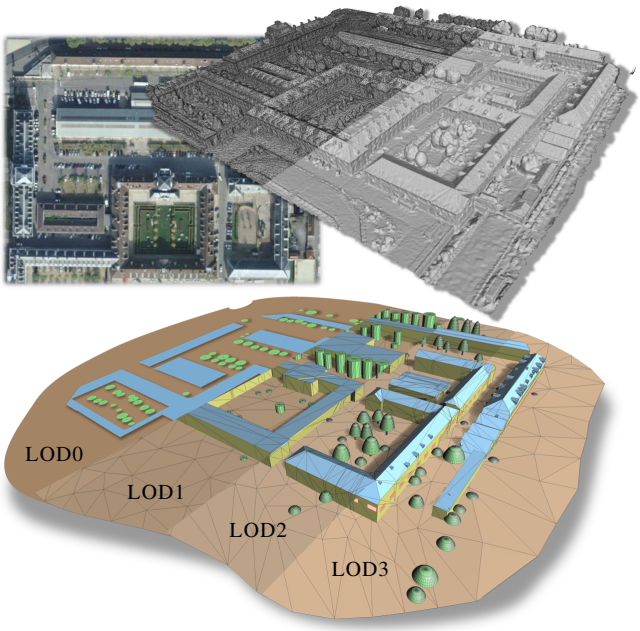

Fig. 1. LOD Generation. Starting from a raw surface mesh (here generated by a multi-view stereo workflow), our approach generates four compact levels of detail that are meaningful, abstracted and enriched with urban semantics.

1. INTRODUCTION

The quest for automated modeling of large scale urban scenes has received an increasing interest in recent years. A first class of approaches apply *procedural modeling* from grammatical rules and a fair amount of user interaction to generate detailed 3D models that are highly semantized [Vanegas et al. 2010]. Another class of approaches, referred to as *urban reconstruction* and focus of the present work, aims at the automated generation of accurate 3D models from physical measurements [Musialski et al. 2013].

The availability of massive airborne data sets at the scale of entire cities has stimulated research on automated methods for urban reconstruction. The quality of the reconstruction may be evaluated through visual inspection, faithfulness to the ground truth when available, or complexity/distortion tradeoff. While LIDAR scans have mostly been used during the last decade, recent advances on fully automated multi-view stereo (MVS) workflows [Acute3D 2014; Autodesk 2014; Pix4D 2014] allow the generation of complex surface triangle meshes, enriched with high resolution textures.

Airborne LIDAR scans exhibit high potential to reconstruct non-vertical elements such as roofs, but often fail to go beyond the 2.5D representation of urban environments. MVS meshes yield real 3D and unprecedented amount of details on vertical components such as facades. Surfaces derived from MVS workflows offer novel opportunities to generate LODs that are controllable via intuitive parameters, and *meaningful* for applications such as interactive navigation, urban planning, computational engineering and video games. Meaningful herein relates to LODs that are coherent across the entire scene, allow for incremental refinement, and provide some level of abstraction. This explains our motivation to go beyond simplification through semantic- and structure-aware reconstruction with LODs (see Fig.1). Note however that MVS meshes are in general less accurate than points generated by LIDAR acquisition systems at similar resolution. In particular, such meshes contain many geometric and topological defects (Fig.2) that require increased robustness for extracting semantic and structural information.

Pierre Alliez acknowledges a Starting Grant from the European Research Council "Robust Geometry Processing" (257474).

DOI 10.1145/XXXXXXX.YYYYYYY
http://doi.acm.org/10.1145/XXXXXXX.YYYYYYY

1.1 Related Work

Our review of previous work covers the four main facets of our problem statement: reconstruction, abstraction, LOD generation and semantic segmentation specific to urban scenes.

Urban reconstruction. In our setup reconstruction amounts to turn the raw input data into LODs of a 3D urban scene composed of watertight buildings in an environment composed of ground and trees. This problem being ill-posed, the state-of-the art ranges from interactive [Arikan et al. 2013] to automated [Poullis and You 2009] through semi-automated approaches [Sinha et al. 2008]. A possible taxonomy of the literature is to distinguish between two types of input data: depth maps and LIDAR point sets.

Depth maps are commonly generated from MVS images. The approaches proposed for generating compact 3D-models of buildings from depth maps proceed, e.g., in 2D through space partitioning [Zebedin et al. 2008] or in 3D through assemblies of cuboids generated by Monte Carlo sampling [Lafarge et al. 2010]. Some approaches combine both ground-based and aerial data to generate more complete representations of urban scenes [Frueh and Zakhor 2003]. In addition to being often hampered with high noise, a major limitation of depth maps is that they prevent distinguishing buildings from high vegetation. LIDAR point set data became popular from the mid-2000 mostly for their accuracy, despite the fact that they are geometrically less structured than depth maps and do not contain any radiometric information. Urban LIDAR data stimulated a series of work mainly focused on parsing building components and extracting building contours.

For LIDAR as well as for depth map data, a popular methodology consists of relying upon 3D planar primitives for roofs and facades [Poullis and You 2009; Lafarge and Mallet 2012], with advances on parsing planes [Toshev et al. 2010] and discovering global regularities among planes [Zhou and Neumann 2012]. The Manhattan World assumption [Coughlan and Yuille 2000] constrains planes to follow only three orthogonal directions. This assumption reduces the solution space to explore as well as the geometry of 3D models [Vanegas et al. 2012]. Both airborne LIDAR scans and depth maps only provide 2.5D representations that prevent modeling the geometry of vertical components.

Some approaches address the urban reconstruction problem by inverse procedural modeling. Based on a grammar and related semantic rules, forward procedural modeling has no equivalent in terms of control over geometric complexity, structure and semantic [Bao et al. 2013]. Impressive results are obtained at the street-view level [Teboul et al. 2010; Martinovic et al. 2012; Riemenschneider et al. 2012]. However, inverse procedural modeling applied to airborne measurement data is still an open problem: state-of-the-art approaches rely on simple grammars and require assumptions such as axis-aligned geometry that do not match our objective [Vanegas et al. 2010].

Abstraction. One step toward an improved control over complexity and structure is a process referred to as abstraction. The latter creates recognizable visual depictions of known objects through compact descriptions involving a handful of characteristic primitives such as curves [Mehra et al. 2009], icons or solids. Abstraction thus goes well beyond shape simplification [Garland and Heckbert 1997] and mesh repairing [Ju 2004] as involves filtering, smoothing, and reinforcing the regular structures. Abstraction is also related to the problem of structure discovery of a scene [Mitra et al. 2013] or of an entire collection of objects [Yumer and Kara 2012]. Abstraction perfectly matches our objective to generate compact descriptions in the form of LODs.

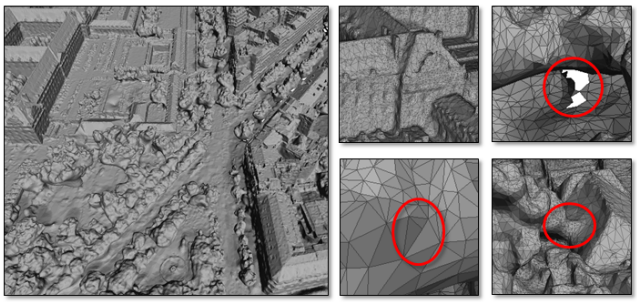

Fig. 2. Raw surface mesh generated by a MVS workflow. The mesh is dense (in the order of 10M triangle facets per city block), semantic-free and defect-laden. It contains many geometric and topological defects such as holes, islands, self-intersections and merging of urban components from distinct classes such as trees and facades.

LOD Generation. Managing LODs is a common topic in geometric modeling [Luebke et al. 2002], but is less common in urban reconstruction [Arefi et al. 2008]. General mesh simplification or approximation approaches are effective but often merge objects of different classes (e.g., a tree and a roof) and fragment structural features such as the boundary of a roof. Most of these approaches rely on a pure geometric error metric and are thus oblivious to semantics and structure of urban scenes. Some error metrics are more feature-preserving than others, which indirectly helps preserve the structure, but the structure itself is scale-dependent and hence can hardly be decoupled from semantic labels specific to urban LODs.

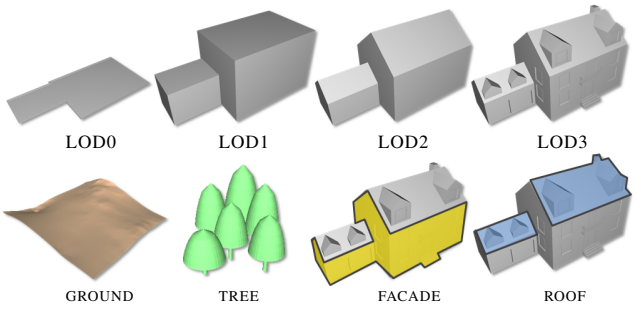

Fig. 3. LODs used by cityGML and semantic labels. Top: LOD0 delineates the footprint of buildings and trees. LOD1 represents the building volume with flat roofs and trees as cylinder icons. LOD2 provides additional details with piecewise-planar roofs and half-ellipsoid icons for trees. LOD3 provides further details such as roof superstructures, doors and windows. Bottom: urban semantic labels used for reconstruction and LOD generation.

Semantic segmentation. Techniques for attempting to bridge the semantic gap have been proposed [Falcidieno and Spagnuolo 1998]. They range from annotation to learning, with the usual dilemmas between interactive vs automated approaches, and supervised vs unsupervised learning. The automated segmentation of surface meshes into parts, too general for our setup, has been well explored [Attene et al. 2006; Shamir 2008; Chen et al.

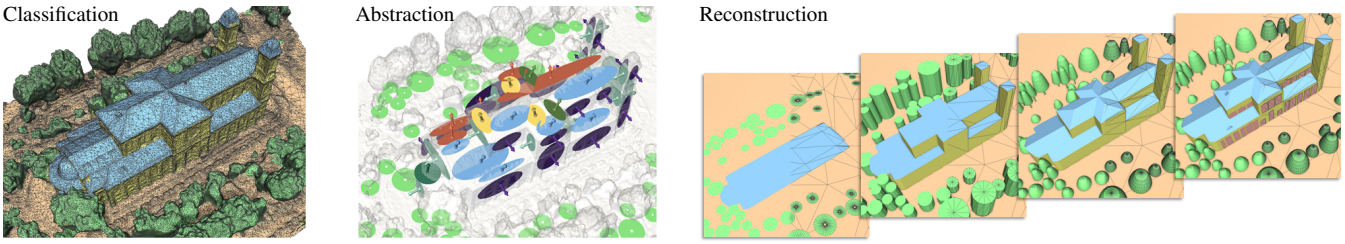

Fig. 4. Main steps of our algorithm. Classification: the input mesh is first segmented into different classes of interest. Abstraction: compact descriptors involving specific icons and planar proxies that are extracted, regularized and filtered according to a LOD formalism. Reconstruction: four LODs are generated from the icons and proxies generated in previous steps.

2009], with clustering or learning [Kalogerakis et al. 2010] as favored methodology. The classification of airborne LIDAR urban scans is also an active research topic [Rottensteiner et al. 2012], with three common classes: building, vegetation and ground. Existing approaches are however not directly applicable to our problem as our input data contain more noise and no additional properties such as echo number or signal magnitude which help distinguishing the classes of interest. Lin et al. [2013] decompose the elements of residential buildings through supervised learning, with however no abstraction nor LODs. In addition, our setup differs as targets unsupervised learning and dense urban scenes with global regularities.

In summary, and in spite of the variety of methods currently available to address each facet of our problem individually, there is a dire need for an automated reconstruction and LOD generation method applicable to dense MVS data measured on large scale urban scenes.

1.2 Positioning and Contributions

In our framework the input data are raw triangle surface meshes, typically generated from multi-view stereo workflows. These meshes are not required to be manifold or watertight. The main objects of interest are buildings and trees, and the structure to discover corresponds to the LODs defined by CityGML [Groger and Plumer 2012], see Fig.3. A given LOD describes both the lower LODs and additional details enriching its structure and geometry. Generating LODs is a crucial advantage when targeting a large range of urban applications.

An important methodological choice when designing a complete urban reconstruction pipeline is the way to associate semantics and geometry. The recent approaches [Haene et al. 2013; Lin et al. 2013] that deal with semantics and geometry simultaneously yield elegant formulations but are not scalable. We instead follow a sequential approach (*semantics-then-geometry*) similar to [Poullis and You 2009; Lafarge and Mallet 2012]. The underlying idea consists in first extracting semantic classes via classification so that (i) the subsequent geometric reconstruction is adapted to each class of interest, and (ii) computational complexity is reasonable even at city scale. Note that existing approaches designed for airborne LIDAR [Poullis and You 2009; Lafarge and Mallet 2012] are not directly applicable to our input data because (i) MVS meshes require high robustness to deal with geometric and topological defects, and (ii) 2.5D shape arrangement processes cannot generate multiple coherent LODs with real 3D.

Our pipeline proceeds with three main steps: semantic-based segmentation of input meshes (§3), abstraction of urban objects via icon extraction and filtering of planar proxies (§4), and reconstruction at four different LODs (§5), see Fig.4.

Our main contributions are as follows:

—A fully automated reconstruction pipeline that departs from existing work by the ability to (i) generate multiple coherent LODs, and (ii) take as input raw surface meshes generated by multi-view stereo workflows;

—Three new technical ingredients that yield robustness to input mesh defects, scalability and efficiency: (i) a feature-preserving Markov Random Field used for classification, (ii) a greedy process for the global regularization of planes with a hierarchical organization of the canonical geometric relationships, and (iii) a min-cut formulation applied to a discrete approximation of a 3D planar arrangement for robust reconstruction.

2. ALGORITHM

The reconstruction algorithm proceeds with three main steps: classification (§3), abstraction (§4) and reconstruction (§5), see Fig.4.

3. CLASSIFICATION

The classification step relies on a Markov Random Field (MRF) in order to distinguish between four classes of urban objects: *ground*, *tree*, *facade* and *roof*. As the classification is unsupervised we rely solely on geometric attributes using the following rationale: *(i) ground* is characterized by locally planar surfaces located below the other classes, *(ii) trees* have curved surfaces, *(iii) facades* are vertical surfaces adjacent to *roofs* and *(iv) roof* are mostly composed of piecewise-planar surfaces.

3.1 Superfacet Clustering

As the input meshes are very dense, classifying each triangle facet through the MRF would lead to unpractical computation times. In a pre-processing step we thus over-segment the input mesh into *superfacets*: sets of connected triangle facets, similar in spirit to the notion of superpixels used for image analysis. Superfacets are obtained by clustering, through region growing, the triangle facets with similar shape operator matrices. More specifically, we estimate the shape operator matrix [Cohen-Steiner and Morvan 2003] for each triangle facet on a local spherical mesh neighborhood of radius R_m, and compare during clustering these matrices via the Frobenius norm. Growing is effective when this distance remains inferior to to a limit value d_l. Fig.5(left) depicts how this clustering procedure identifies the nearly planar components and preserves the sharp features.

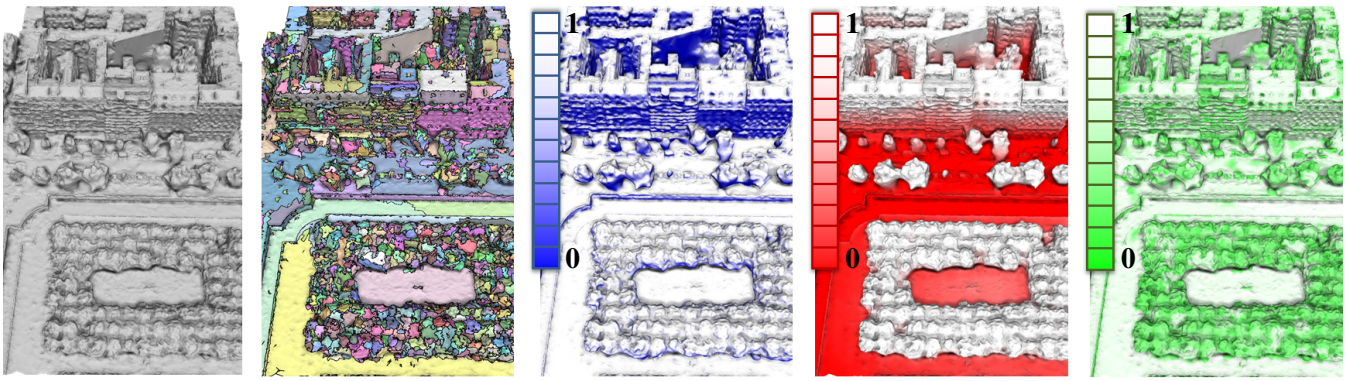

Input mesh Superfacets Horizontality Elevation Planarity

Fig. 5. Superfacet clustering and geometric attributes used for classification. Superfacet clustering produces nearly planar patches that preserve sharp creases and reduce the complexity of the classification problem. The three considered geometric attributes provide distinct and complementary information to classify the urban object of interest.

3.2 Geometric Attributes

Three geometric attributes are computed for each triangle facet f_i of the input mesh:

—The **elevation** attribute a_e is defined as a function of the relative height (z coordinate) of the triangle facet centroid, denoted by z_i:

$$a_e(f_i) = \sqrt{\frac{z_i - z_{min}}{z_{max} - z_{min}}}, \quad (1)$$

where $(z_{min}; z_{max})$ denotes the height range of all triangle facet centroids located within a local spatial neighborhood. The square root ensures that small values of relative height get a larger elevation attribute. The size of the neighborhood, set by default to 40 yards, must be sufficiently large to meet ground components and sufficiently small to gain resilience to hilly environments.

—The **planarity** attribute a_p denotes the planarity of the superfacet containing f_i, derived from the so-called surface variation [Pauly et al. 2002]:

$$a_p(f_i) = 1 - \frac{3\,\lambda_0}{\lambda_0 + \lambda_1 + \lambda_2}, \quad (2)$$

where λ_0 denotes the minimum eigenvalues of the covariance matrix computed in closed form over all triangle facets of the superfacet containing f_i. Each eigenvalue measures the variance of the superfacet along the corresponding eigenvector. The variation measures how much the superfacet deviates from the local tangent plane: the planarity is thus 1 for a perfectly planar superfacet, and 0 for an isotropic superfacet with three identical eigenvalues.

—The **horizontality** attribute a_h measures the deviation of the unit normal $\mathbf{n}_i$ to triangle facet f_i with respect to the vertical axis:

$$a_h(f_i) = |\mathbf{n}_i \cdot \mathbf{n}_z|, \quad (3)$$

where $\mathbf{n}_z$ denotes a unit vector along the Z coordinate axis.

From these geometric attributes defined for each triangle facet, all taking values within $[0, 1]$, we compute the geometric attribute for each superfacet as the area-weighted sum of the geometric attributes of its triangle facets. We compute similarly the normals of superfacets. Figure 5 illustrates the superfacet clustering and geometric attributes on a part of a urban scene.

3.3 Markov Random Field

From the geometric attributes computed per superfacet, a Markov Random Field is used to label each superfacet with one of the four classes: $\{$*ground*, *tree*, *facade*, *roof*$\}$. The defects of the raw input mesh require a regularized global optimization process offered by MRF which adds contextual as well as spatial consistency to the classification. More specifically, we use a MRF with pairwise superfacet interactions. The quality of a label configuration l is measured by energy U:

$$U(l) = \sum_{i \in S} D_i(l_i) + \gamma \sum_{\{i,j\} \in E} V_{ij}(l_i, l_j) \quad (4)$$

where D_i and V_{ij} denote the unary data term and propagation constraints respectively, balanced by parameter $\gamma > 0$. S denotes the set of superfacets. E denotes all pairs of adjacent superfacets, two superfacets being adjacent if they share at least one edge in the input mesh. The data term combines the above-described attributes weighted by the area A_i of the superfacet i:

$$D_i(l_i) = A_i \times \begin{cases} 1 - a_p \cdot a_h \cdot \overline{a_e} & \text{if } l_i = \textit{ground} \\ 1 - \overline{a_p} \cdot a_h & \text{if } l_i = \textit{tree} \\ 1 - a_p \cdot \overline{a_h} & \text{if } l_i = \textit{facade} \\ 1 - a_p \cdot a_h \cdot a_e & \text{if } l_i = \textit{roof} \end{cases} \quad (5)$$

where $\overline{a_\cdot} = 1 - a_\cdot$. The pairwise interaction V_{ij} between two adjacent superfacets i and j favors label smoothness away from sharp creases:

$$V_{ij}(l_i, l_j) = C_{ij} \cdot w_{ij} \cdot 1_{\{l_i \neq l_j\}}, \quad (6)$$

where $1_{\{\cdot\}}$ denotes the characteristic function, and C_{ij} denotes the length of the interface between superfacets i and j (sum of interface edge lengths). Weight w_{ij} is introduced to lower the label propagation over sharp creases that often appear when two classes meet (e.g., for trees adjacent to facades, see Fig. 6). w_{ij} is defined as the angle cosine between the estimated normals of two superfacets. As the unary data term and pairwise potential are weighted by the superfacet areas and interface lengths, this energy formulation behaves similarly to a triangle facet-based energy with grouping constraints. An approximate solution to this energy minimization problem is solved through the $\alpha - \beta$ swap algorithm [Boykov et al. 2001].

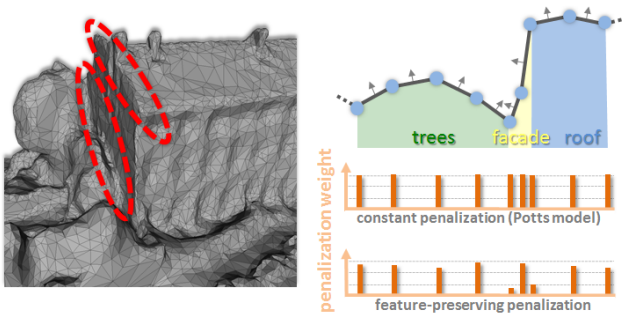

Fig. 6. Feature-preserving regularization. Contrary to the traditional Potts model [Li 2001], our pairwise interaction term softly penalizes label propagation over sharp creases by taking into account the normal variation of the superfacets.

3.4 Semantic Rules

The aforementioned geometric rationale alone is not sufficient to solve the ill-posed classification problem. Two types of errors frequently occur when dealing with complex urban scenes: *(i)* roof superstructures such as chimneys or dormer-widows may be wrongly labeled as *tree*, these elements being too small and irregular to be considered locally planar, and *(ii)* vertical components of large trees may be labeled as *facade*. We thus add the following semantic rules:

—*Rule 1.* superfacets labeled as *tree* and adjacent to only superfacets labeled as *roof* are re-labeled *roof*. This rule relies on the common assumption that large trees are not located on top of roofs.

—*Rule 2.* superfacets labeled as *facade* and adjacent to superfacets labeled as *tree* and *ground* are turned to *tree*.

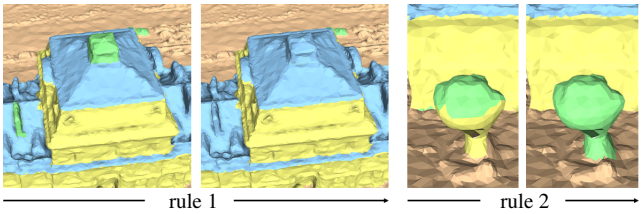

Fig. 7. Semantic rules. Labeling small roof superstructures as *tree* (left) and vertical parts of trees as *facade* (right) are two common errors made during the MRF-based classification. Adding two semantic rules correct most of these errors by reinforcing the contextual coherence of the urban scene. Color code: roof (blue), facade (yellow), ground (brown) and trees (green).

As illustrated by Fig.7 and 8, these two semantic rules bring higher contextual coherence to the semantic labeling, in particular in presence of small irregular roof superstructures and trees with cylindrical shapes. We evaluate in our experiments that these rules impact only around 2% of the area of the classified mesh. Finally, after classification we decompose the scene into connected components: isolated buildings or blocks of connected buildings are extracted by searching for connected components of superfacets labeled as $roof$ and $facade$. Isolated trees and forests are extracted using a similar process. Such decomposition greatly reduces the complexity of the reconstruction step as each connected block of buildings or trees is reconstructed independently.

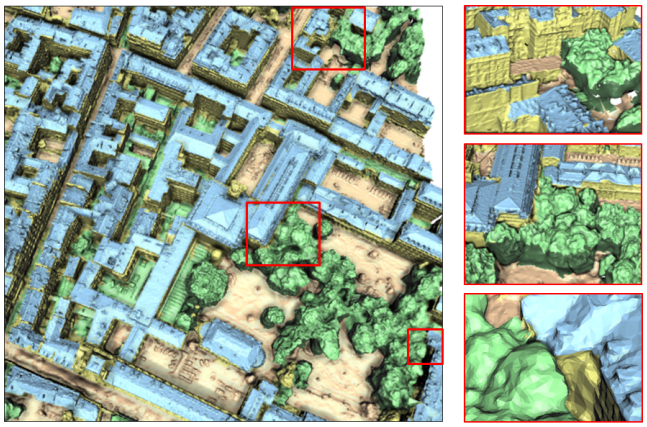

Fig. 8. Classification into four classes of urban elements. The regularizing term of the energy as well as the semantic rules improve spatial consistency. The close-ups depict how roofs and facades, as well as trees adjacent to facades, are adequately separated.

4. ABSTRACTION

From the superfacets classified in §3 the abstraction step creates compact descriptions involving characteristic icons and planar proxies. Compact descriptions are obtained by geometric and structure simplification through planar shape approximation and regularization, iconization and LOD-based filtering. Remind that superfacets are classified into four classes: *ground*, *tree*, *facade* and *roof*, the latter containing roof superstructures. A key idea behind our approach is to specialize the abstraction and reconstruction steps to these classes as well as to the LODs, such that, e.g., trees are represented by icons instead of attempting to reconstruct them with planar proxies. In addition, regularization is our means to improve scalability and robustness of the reconstruction step.

The classes are abstracted as follows:

—**Ground** is represented by a 2D Delaunay triangulation lifted in 3D with a natural neighbor interpolation of the maximum elevation attribute of the input mesh superfacets labeled as *ground* (see §3).

—**Facades and roofs** are approximated by a set of planar proxies with reinforced regularities, these proxies being used as input to the final watertight reconstruction step (§5). We restrict ourselves to planar proxies as planar surfaces cover on average 80% of urban areas, and are amenable to effective abstraction and reconstruction for LOD generation.

—**Roof superstructures, facade components and trees** are abstracted through iconization on distinct depth maps. We do not approximate roof superstructures and facade components with planar proxies due to the limited resolution of airborne MVS meshes (typically as only a few triangle facets for a chimney or a window). For a similar reason there is no specific superstructure class, and, e.g., chimneys are re-labeled from *tree* to *roof* during classification (see §3). Tree icons are parametric shapes invariant by rotation along Z-axis, similar to [Verdie and Lafarge 2014].

The icons and regularized proxies are then filtered through LOD generation, before reconstruction.

4.1 Planar Proxies

We first identify a set of nearly planar superfacets by selecting the ones labeled as *roof* or *facade*, with a high planarity attribute a_p and a minimum large area (we impose $a_p > t_p$ and area A larger than A_{min} where t_p and A_{min} are two model parameters). For each near-planar superfacet we compute its least-squares fitting plane, referred to as superfacet proxy. We then improve globally the regularity of these proxies by altering their orientation and position so as to reinforce their canonical geometric relationships. Departing from other approaches such as GlobFit [Li et al. 2011] or LIDAR-specific algorithms [Zhou and Neumann 2012], we adopt a *detection-then-regularization* strategy with a single iteration in order to favor scalability and low running times. For instance, less than one second is required to regularize proxies shown by Fig.9 instead of ten minutes for Globfit. The main idea is to organize the geometric relationships hierarchically then regularize the proxies in one step via a greedy process. In addition, we introduce a novel Z-symmetry geometric relationship relevant for abstracting building roofs.

Geometric relationships. Denote by P_1 and P_2, two proxies with respective unit normals $\mathbf{n}_1$ and $\mathbf{n}_2$, and centroids c_1 and c_2. We define four canonical relationships under an orientation tolerance ϵ and an Euclidean distance tolerance d:

—*Parallelism.* P_1 and P_2 are ϵ-parallel if $|\mathbf{n}_1 \cdot \mathbf{n}_2| \geq 1 - \epsilon$;

—*Orthogonality.* P_1 and P_2 are ϵ-orthogonal if $|\mathbf{n}_1 \cdot \mathbf{n}_2| \leq \epsilon$;

—*Z-symmetry.* P_1 and P_2 are ϵ-Z-symmetric if $||\mathbf{n}_1 \cdot \mathbf{n}_z| - |\mathbf{n}_2 \cdot \mathbf{n}_z|| \leq \epsilon$, where $\mathbf{n}_z$ is the unit vector along the vertical axis;

—*Coplanarity.* P_1 and P_2 are d-ϵ-coplanar if they are ϵ-parallel and $|d_\perp(c_1, P_2) + d_\perp(c_2, P_1)| < 2d$, where $d_\perp(c, P)$ denotes the orthogonal distance between point c and proxy P.

The first three relationships are related to the proxy orientations, and coplanarity is a specific instance of parallelism with an additional relative positioning constraint. The notion of Z-symmetry matches the common assumption that connected components of roofs tend to share similar slope values. For our urban context the rotational symmetry [Li et al. 2011; Zhou and Neumann 2012] is too general. In addition, Z-symmetry is detected with linear operations while rotational symmetry involves a quadratic complexity.

Detection of regularities. Global regularities are detected via a hierarchical decomposition. Parallelism relationships form the reference layer - referred to as layer 1- of this hierarchy: we cluster the proxies which are ϵ-parallel into parallel clusters, and compute the average orientation of each cluster. The upper layer - referred to as layer 2 - is formed by detecting orthogonality and Z-symmetry relationships among the parallel clusters. An orthogonality graph is constructed with one node per parallel cluster, and one edge between two nodes that are ϵ-orthogonal. We also cluster the parallel clusters which are ϵ-Z-symmetric into Z-symmetric groups, and compute the average angle of each group with respect to the Z-axis. A lower layer - referred to as layer 0 - is finally created via the coplanarity relationship: we decompose each parallel cluster into sets of proxies that are d-ϵ-coplanar, and compute the average centroid for each set of coplanar proxies. Note that all aforementioned averaging processes are weighted by the area of each proxy, the area of each proxy being defined by the total area of its associated superfacets. Such hierarchical organization is efficient as we avoid performing a costly pairwise analysis of the different relationships among proxies. Fig.9 illustrates the hierarchical organization used to detect regularities.

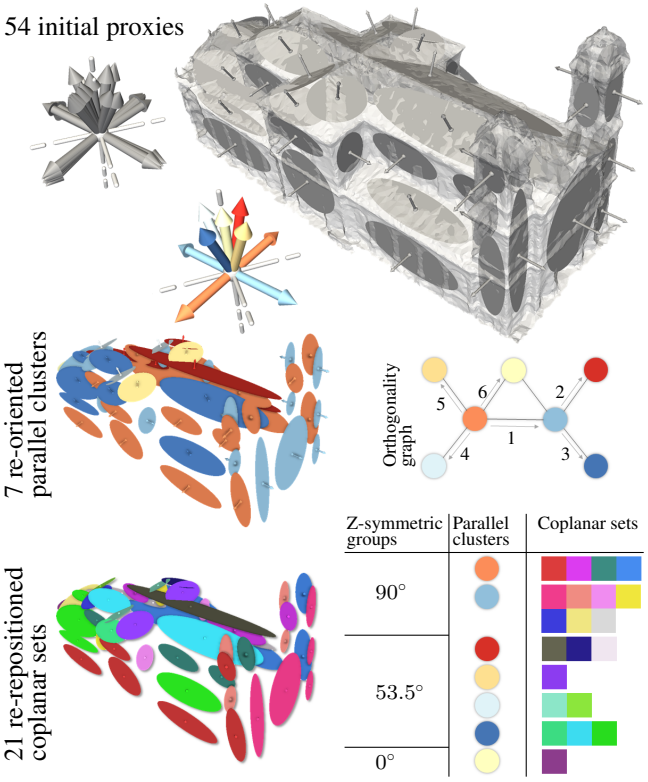

Fig. 9. Regularization of proxies. The 54 planar proxies detected from the input mesh (top) are separated into 7 parallel clusters, which are themselves divided into 3 Z-symmetric clusters. The numbers on edges of the orthogonality graph denote the greedy propagation order of geometric constraints over parallel clusters. Re-oriented parallel clusters are then decomposed into 21 coplanar sets. The space partition constructed from the 21 planes contains 291 cells instead of 1,847 cells with the 54 initial planes.

The regularization step operates on clusters of proxies, and comprises two steps: re-orientation and re-positioning.

Re-orientation. Parallel clusters are re-oriented through propagating geometric relationships into the orthogonality graph. Denote respectively by source and target node a pair of nodes altered by the propagation. The initial orientation of the target node is altered by constraining its normal to match the relationships of (i) orthogonality with respect to the source node, and (ii) Z-symmetry if the node has been clustered into a Z-symmetric group. We distinguish between three cases:

—*Case A: both relationships are active.* There is in general a unique orientation that satisfies both relationships. It may occur that no solution exists due to contradicting relationships: the target node is then not re-oriented.

—*Case B: only the orthogonality relationship is active.* We re-orient the target node in accordance to the orientation orthogonal

to the source node in the hierarchy, that best aligns to its initial orientation.

—*Case C: only the Z-symmetry relationship is active.* This occurs when a node has no parent in the hierarchy, i.e., when it is the root node of the orthogonality graph. We re-orient the target node in accordance to the orientation satisfying the Z-symmetry constraint that best aligns to its initial orientation.

These three cases are illustrated by Fig.10 with a representation on the unit sphere. To prevent from large deviations, we perform a re-orientation only when the dot product between the initial and the re-oriented normals is lower than $1-\epsilon$. The greedy propagation in the orthogonality graph proceeds from large to small nodes, the size of a node being defined by the total area of its proxies. Such loop-free propagation tends to reduce contradictions between relationships and gives more confidence to the larger nodes.

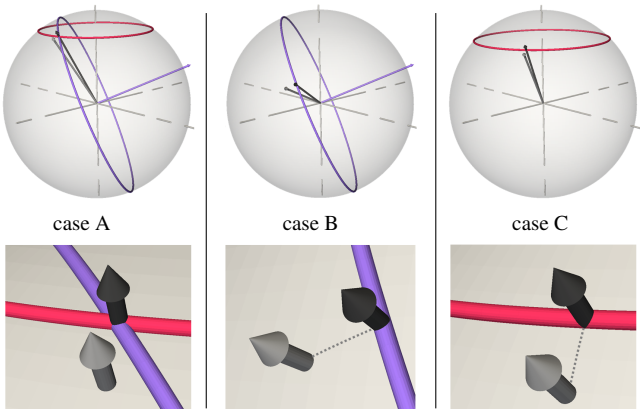

Fig. 10. Proxy re-orientation. The orthogonality (respectively Z-symmetry) relationship is represented by a blue (resp. red) circle on the unit sphere. To satisfy both relationships (case A), the initial orientation (grey arrow) must be relocated to the intersection with the circle. When only one relationship is active (cases B and C), the initial orientation is projected orthogonally onto the circle. The black arrow corresponds to the new orientation.

Re-positioning. For each set of coplanar proxies, the centroid of each proxy is translated along the line supporting the proxy normal so that the average centroid of the coplanar set is contained within the proxy plane.

4.2 Iconization

The iconization step is devised to abstract trees, roof superstructures and facade elements. For these three types of icons, we adopt a two-step strategy illustrated in Fig.11. Elements of interest are first located from depth maps, and then abstracted by 3D icons that are fitted to the input mesh. Icons of trees are used at the four LODs, whereas roof superstructure and facade icons are only used at LOD3.

For trees we first construct a depth map by rasterizing in an image the input mesh in the XY coordinate plane and taking as height value the maximum elevation attribute restricted to superfacets labeled as *tree*. We greedily extract the local maxima of this map by a watershed algorithm in order to locate the center of each tree icon in the XY plane, and fit the best half ellipsoid to the map while keeping the center fixed, similar to [Lafarge and Mallet 2012].

For roof superstructures, which mainly correspond to chimneys, dormer-windows and small roof extensions, we construct a depth map by rasterizing in an image the difference between the maximum elevation attribute restricted to superfacets labeled as roof, and the LOD2 model generated by the watertight reconstruction process described in Section §5. We then locate the center of each superstructure icon similarly to the tree icons, and fit a 3D template icon made of two superimposed parallelepiped.

For facade elements such as windows and doors, the resolution of MSV meshes is not sufficient to extract individual elements. Departing from the inverse procedural modeling approach [Teboul et al. 2010; Martinovic et al. 2012; Riemenschneider et al. 2012], we constrain the elements of a facade to follow a regular grid layout. For each facade reconstructed at LOD2 we first build a rasterized depth map measuring the distance between superfacets labeled as facade and the facade of LOD2. We then estimate both row and column spacing of the grid layout, as well as the position of its first element, by searching for the local maxima of the depth map. For each grid element we then assign a label *occupied* or *empty*. A Markov Random Field with an energy formulation defined in Eq.4 is then used to assign labels via non-local optimization. More specifically, a common Potts model [Li 2001] is used to model pairwise interaction in order favor similar label assignments in local neighborhoods defined by 4-connectivity in the grid layout. The unary data term models the coherence between a label and the depth map. Denote by d_{center} the depth value at the grid element center. We define $D_i = d_{center}$ if *empty* and $D_i = 1 - min(1, d_{center})$ otherwise. The energy is minimized via a graph-cut algorithm [Boykov et al. 2001]. For each grid element labeled as *occupied* we then classify it as either a door or a window. A grid element is classified as a door when it is located at the bottom row of the grid and contains a minimum average depth value (set to 10cm by default). All other occupied elements are classified as windows.

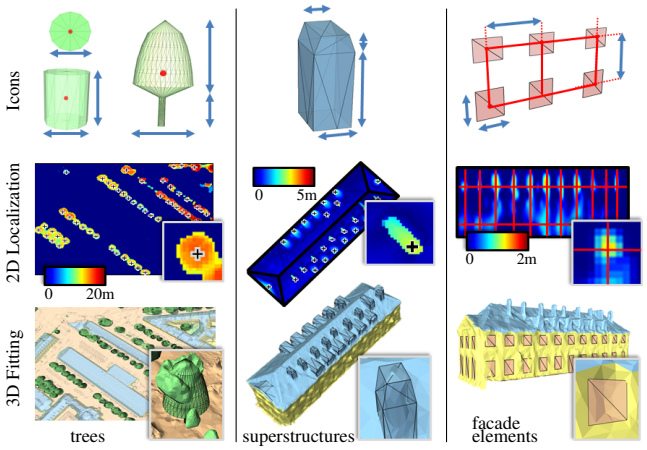

Fig. 11. Iconization. Each icon is defined by up to 5 parameters. The three types of icons correspond to different resolution requirements for the 2D localization and 3D fitting steps (see scale of depth maps, middle row).

4.3 LOD Generation

The LOD generation step proceeds by filtering the regularized proxies and abstracting the icons, in accordance to the urban LODs used by CityGML:

—LOD0: the ground mesh is not used as the representation is planar. Trees are depicted as discs computed as vertical projection of tree icons, and buildings are depicted by 2D regions bounded by polylines computed only from the abstracted proxies labeled as *facade* using a 2D instance of the min-cut formulation (§5). Superstructures are omitted.

—LOD1: ground mesh, enriched with vertical cylinders for trees and a LOD0-building elevated in 3D with horizontal proxies as roofs whose height is defined as the median of associated superfacet heights.

—LOD2: ground mesh enriched with tree icons and buildings reconstructed (§5) with all proxies to generate piecewise-planar roofs.

—LOD3: LOD2 enriched with roof superstructures and facade elements.

5. RECONSTRUCTION

The final reconstruction step turns the proxies regularized and filtered in previous step into watertight buildings. For each connected component of buildings identified in §3, a 3D arrangement of planes provides us with a means to assemble the planar proxies into well-behaved surfaces: watertight and free of self-intersection. When combined with global regularization, LOD filtering and min-cut, it furthermore generates lightweight polygon meshes that preserve the structural components of the scene at the chosen LOD, and completes missing parts of the scene in a plausible manner.

5.1 Discrete 3D Arrangements

Even when restricting it to each building component, computing the complete, exact arrangement leads to very high computational complexity (we experimented with scenes containing hundreds of building components, each containing on average hundred planes). Previous work based on arrangements attempted to reduce complexity by restricting the arrangements to axis-aligned planes [Furukawa et al. 2009], creating multi-layers of 2D arrangements of lines [Oesau et al. 2014] or computing a two-level hierarchy made up of a rectilinear volumetric grid combined with a convex polyhedral cell decomposition [Chauve et al. 2010]. The approaches are either too restrictive or algorithmically too complex, exceeding half an hour when dealing with only few hundred planes. Observing that only a very small subset of the faces of the arrangement contribute to the output after solving for a min-cut surface, we postpone the exact geometric computation operations to the final surface extraction step after min-cut solve. We rely instead on a transient discrete approximation of the arrangement so as to avoid the compute-intensive exact geometric operations required to insert each plane into the arrangement.

For each subset of the input mesh associated to a building component we first compute an object-oriented bounding box B. We then sample uniformly B by placing anchors points at all corners of a uniform grid aligned to B. Each of these anchors is enriched with two attributes:

—A binary flag that specifies whether the anchor is estimated to be inside or outside the inferred building. This flag is guessed by casting rays and counting the intersection parity of these rays against the input mesh. If the number of rays with odd (resp. even) intersections is higher, an inside (resp. outside) flag is assigned to the anchor. Five rays have shown sufficient in all experiments: four towards the upper corners of B and one towards the barycenter of these corners. For input meshes highly corrupted with spurious holes, a more global approach [Zhou et al. 2008] would be better suited.

—An integer that denotes the index of the cell of the planar arrangement containing the anchor.

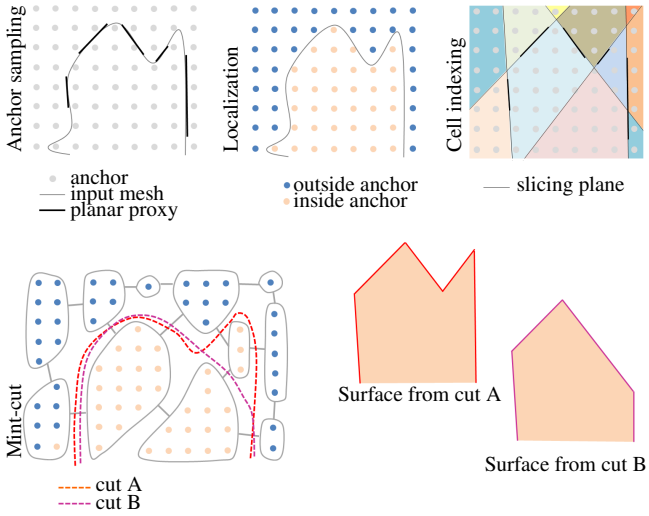

Fig. 12. Discrete arrangement. Each anchor is associated to (i) a Boolean flag defining its inside/outside localization guess with respect to the inferred building, and (ii) the index of its containing cell (top). A cut in the graph constructed from cell adjacency separates inside from outside cells, and defines a surface as the set of interface facets between volumes. Cuts A and B depict two plausible results. Cut A gives importance to the initial inside/outside localization guess (low β parameter in Eq.7) whereas cut B favors smaller surface areas (high β parameter).

Instead of computing the exact geometry of the arrangement cells the approximate arrangement of planes is constructed solely via an arrangement binary tree and the anchor cell indices. More specifically, we greedily insert the 6 planes of B, then the planar proxies, while refining the binary tree in which each node refers to a cell. The anchor cell indices are updated after each plane insertion: this operation corresponds to the insertion of a new layer of nodes into the binary tree.
The anchors are also used to compute via quadratures approximate geometric attributes (volume of cells, area of facets) that are required by the subsequent min-cut formulation. Fig.12 depicts a set of anchors at work for surface reconstruction.

5.2 Min-Cut Formulation

For each arrangement a min-cut formulation is used to find an inside/outside labeling of the cells, the output surface being defined as the interface facets between inside and outside. Consider a graph $(\mathcal{C}, \mathcal{F})$ where $\mathcal{C} = \{c_1, \ldots, c_n\}$ denotes the nodes relating to the cells induced by the space partition, and $\mathcal{F} = \{f_1, \ldots, f_m\}$ denotes edges relating to the facets separating all pairs of adjacent cells. A cut in the graph consists of separating the cells $\mathcal{C}$ into two disjoint sets $\mathcal{C}_{in}$ and $\mathcal{C}_{out}$. The edges between $\mathcal{C}_{in}$ and $\mathcal{C}_{out}$ correspond to a set of facets forming a surface $\mathcal{S} \subset \mathcal{F}$.

In order to quantize the quality of the solution, i.e., the surface $\mathcal{S}$ induced by the cut $(\mathcal{C}_{in}, \mathcal{C}_{out})$, we introduce the following cost

function C:

$$C(\mathcal{S}) = \sum_{c_k \in \mathcal{C}_{out}} V_{c_k}\, g(c_k) + \sum_{c_k \in \mathcal{C}_{in}} V_{c_k}\, (1 - g(c_k)) + \beta \sum_{f_i \in \mathcal{S}} A_{f_i}, \tag{7}$$

where V_{c_k} denotes the volume of cell c_k, $g(c_k)$ denotes the function estimating the label likelihood of cell c_k with respect to the ratio of its inside/outside anchors, and A_{f_i} denotes the discrete area of facet f_i . The first two terms of the cost function C are data terms whereas the third term weighted by parameter $\beta \geq 0$ acts as a regularization term in order to favor solutions with small area. The optimal cut minimizing the cost $C(\mathcal{S})$ is found via the max-flow algorithm [Boykov and Kolmogorov 2004].

Function $g(c_k)$, defined in the interval $[0, 1]$, quantizes the coherence of assigning label *inside* to cell c_k with ratio r_{in} of inside anchors contained in c_k:

$$g(c_k) = \frac{(2r_{in} - 1) \times |2r_{in} - 1|^{\alpha} + 1}{2}, \tag{8}$$

where α denotes a parameter tuning the data sensitivity of function g, as illustrated by Fig.13.

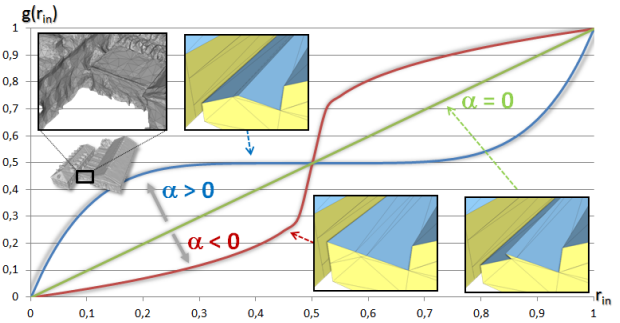

Fig. 13. Behavior of label likelihood function g with respect to r_{in}. Choosing $\alpha = 0$ yields a linear penalization function of ratio r_{in}. Increasing α yields a constant penalization when ratio r_{in} is around 0.5. The impact of the data term in the cost function is reduced, favoring surfaces with small area (top). To the contrary, if $\alpha < 0$, g strongly penalizes cells whose labels are inconsistent with the ratio r_{in}.

The optimal cut corresponds to a subset of facets separating the inside and outside cells, as depicted by Fig.12. The final geometry of these interface facets is then computed with exact arithmetic by intersecting the set of corresponding planes from the binary tree. By construction each interface facet is thus a planar convex polygon. For LOD0 and LOD1 we create a 2D instance of such discrete arrangement and min-cut formulation by sampling a single horizontal layer of anchors. In some rare cases a cell is free of anchors. Such a cell, referred to as an *empty cell*, is not taken into account in the cost function C as its discrete volume is null. This situation may arise when the cell is thin compared to the anchor spacing. The anchor spacing must also be not too short in order to reach practical performance and memory consumption. Empty cells are rare in practice thanks to the plane regularization process which limits the number of thin cells, in particular when we constrain the anchor spacing to be lower than the Euclidean distance tolerance d, as illustrated by Fig 14. In all experiments shown the default value for the anchor spacing is set to 0.5 yards.

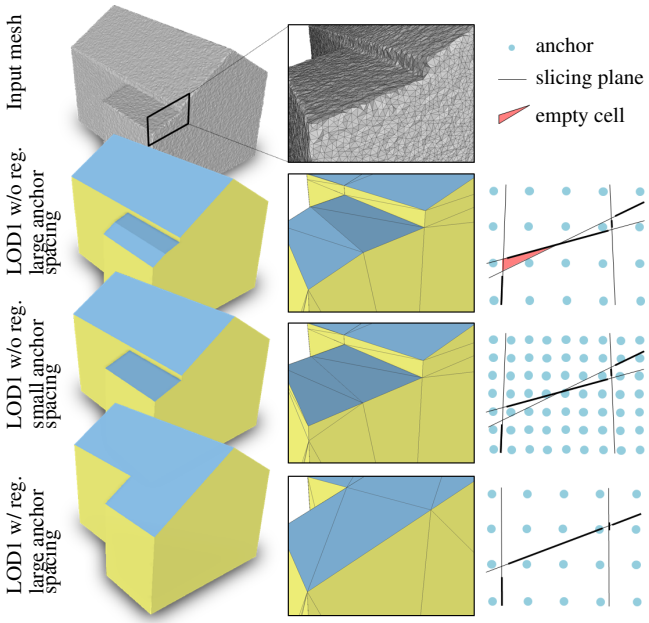

Fig. 14. Anchor spacing and empty cells. The empty cells, *i.e.*, the small cells which do not contain any anchors, can lead to omitting thin volume elements in the output surface (second row). In order to reduce their occurrence the anchor spacing can be diminished (third row). The plane regularization process is also useful to avoid small cells as less plane intersections occur (bottom): output surface is less detailed but running times are not impacted contrary to the anchor spacing reduction option.

Table I. Parameters used in all experiments shown, except for Fig. 13 and 17 which illustrate the impact of various parameters.

	Parameters	Value
Classification	Mesh neighborhood radius R_m	2 (in yards)
	Growing criterion limit distance d_l	0.5 (in yards)
	Pairwise potential weight γ	0.5
Abstraction	Planar proxy tolerance t_p	0.7
	Planar proxy minimal size A_{min}	10 (in square yards)
	Orientation tolerance ϵ	0.05
	Euclidean distance tolerance d	0.5 (in yards)
Reconstruction	Anchor spacing	0.5 (chosen as d, in yards)
	Data sensitivity α	0
	Regularization weight β	1

6. RESULTS

Our algorithm is implemented in C++ using the CGAL library, an $\alpha - \beta$ swap and a max-flow library [Boykov and Kolmogorov 2004; Boykov et al. 2001]. All timings are measured on an Intel Core i7 clocked at 2GHz. We experiment with real-world meshes generated by state-of-the-art multi-view stereo workflows (Acute3D Smart3DCapure and Autodesk 123DCatch) as well as with defect-free meshes used to evaluate robustness and accuracy. The parameters of the algorithm and their default values are summarized in Tab. I. The number of parameters is large, but this is the price to pay for such a complete system combining semantic segmentation, abstraction and LOD reconstruction of urban scenes in an unsupervised manner. Note also that the default values of these parameters, used for all shown experiments, are

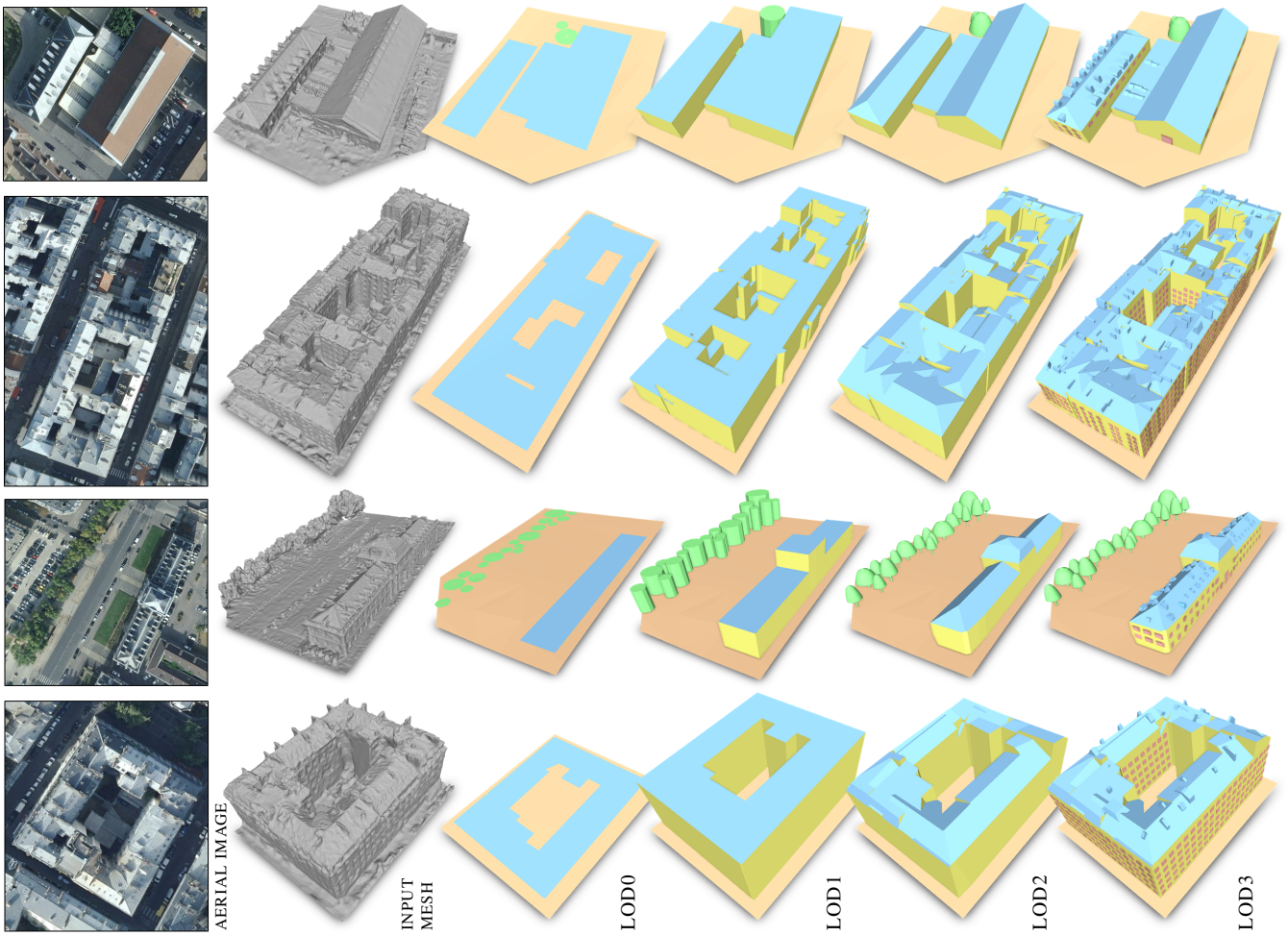

Fig. 15. Reconstruction and LOD Generation. First row: on this simple residential scene all facades and roofs are well classified and the Z-symmetry relationships between the two types of roof (2 and 4 slopes) enables abstraction. Second row: on this dense urban component each roof is simple but all roofs form a complex arrangement as the buildings have been built at different times with little coherence. Third row: on this architectural building both Z-symmetry and orthogonal relationships cooperate to abstract the central part of the roof. Fourth row: this building contains complex and thin roof superstructures. Despite a limited accuracy of the input MVS mesh our method recovers the main facades and roofs, and most superstructures.

Table II. Running times and output complexity. The time required for reconstruction LOD2 and LOD3, as well as for extracting LOD0 and LOD1 are similar as the time required for iconization and height filtering is negligible. The complexity refers only to the number of polygon facets of the building models at LOD2, the trees and superstructures being omitted.

Input mesh	Classification	Planar proxies	Iconization	LOD1 reconstruction	LOD2 reconstruction	Model complexity
Church (59K triangle facets, Fig.17)	5s	1.5s	2s	41s	198s	190 facets
Building block (170K triangle facets, Fig. 15, 2nd row)	7s	1.1s	1.1s	21s	137s	456 facets
Invalides district (11M triangle facets, Fig. 16)	55s	95s	36s	17min	112min	175K facets

stable on a large range of inputs. Fig.15 illustrates our algorithm at work on various types of urban scenes ranging from residential houses to dense urban blocks through architectural buildings. The reconstructions match our initial goal to generate meaningful levels of details: the semantic labels are recovered, the structures are preserved and the details are coherent across the scene.

Scalability and Performances. Our pipeline digests input meshes with several million triangle facets. On average a block of buildings is fully processed in around 30 seconds for LOD1 and 3 minutes for LOD2. Fig.16 depicts a variable density urban scene covering 1km square of Paris with 235 building components, 3.3K roofs and 1.3K trees. For this complex model the total running time is less than 20 minutes for LOD1 and around 2 hours for LOD2 (175K facets), with a sequential implementation of the plane arrangement per block. The LOD-reconstructions are the most time-consuming operations, in particular the LOD2-reconstruction where the plane arrangement is performed in 3D with all the

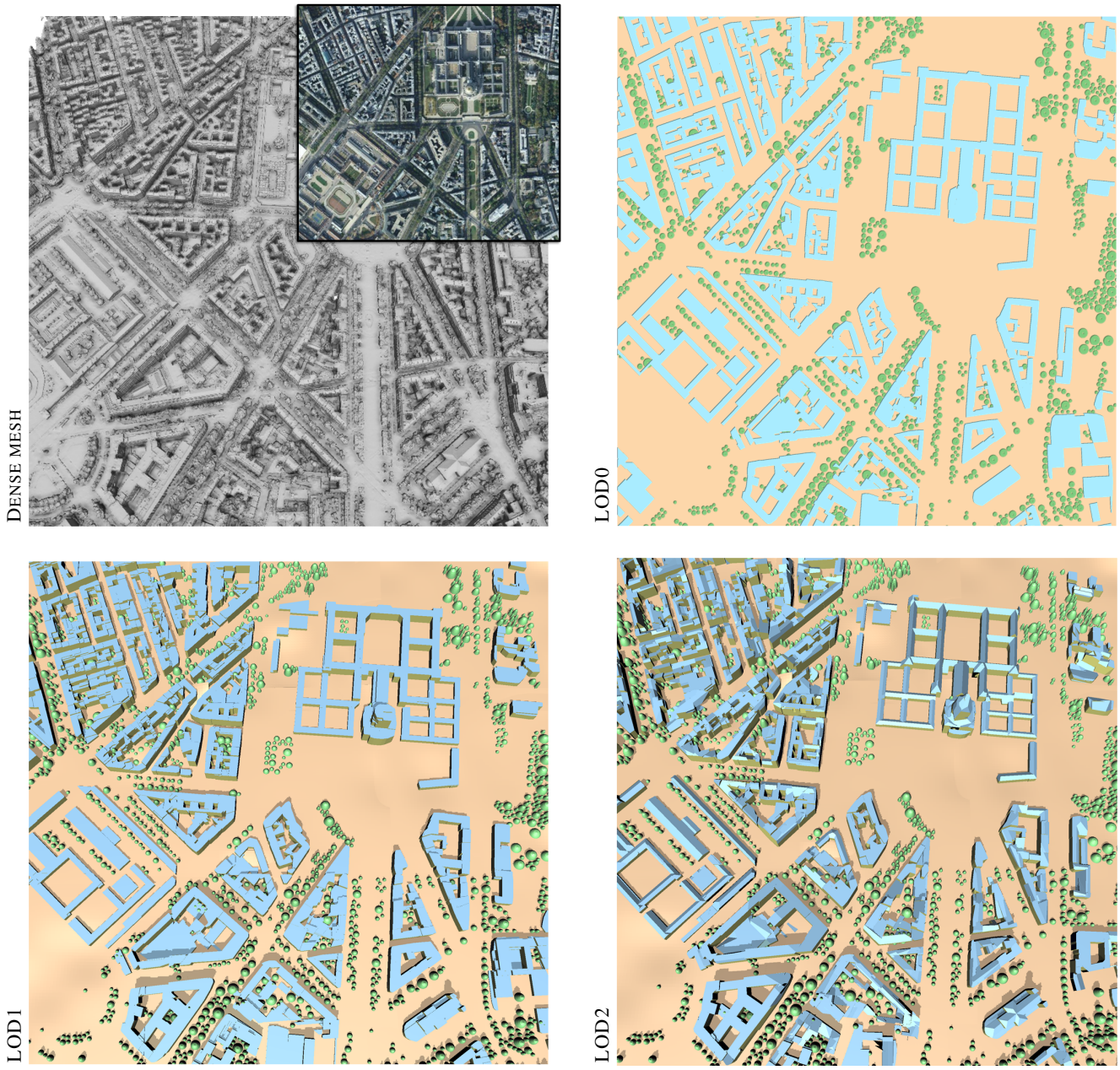

Fig. 16. Reconstruction on large-scale urban scene. The input mesh (11M triangle facets) was generated from 600 airborne images. LOD1 and LOD2 comprise 10K and 175K polygon facets respectively, excluding tree and ground meshes.

proxies. LOD3 is not shown because superstructures are not observable at this scale. Tab.II lists some models and associated numbers.

Robustness. Cases that challenge the robustness of our algorithms include input meshes with insufficient density and defects such as noise, holes and overlaps. Fig.15(fourth row) shows that small scale roofs may not be reconstructed in LOD2 but are recovered in LOD3 as roof superstructures. Imperfect input data often lead to over- or under-detected planar proxies. We observe that over-detection is often compensated by the proxy regularization procedure that merges nearly-coplanar proxies. Under-detection however leads to very few proxies as observed on free-form architectural buildings, and hence to an overly abstracted reconstruction. Nevertheless, in the worst case where no proxies are detected for a building component, the output LOD is abstracted as its bounding box. Data that challenge the classification step include merged objects such as a tree touching a facade, and clutter elements such as cars or hedges digested by the four classes of interest. The regularization term of the energy

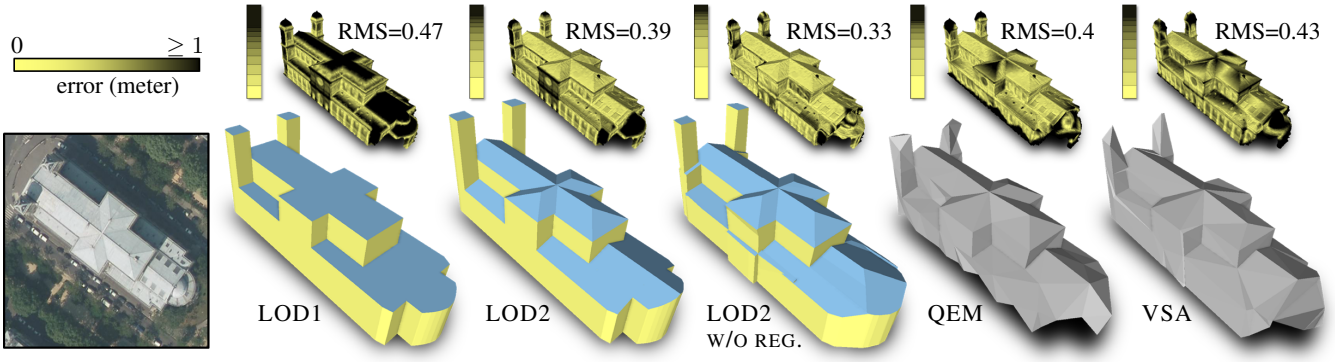

Fig. 17. Geometric accuracy and structure-awareness. We compare the LODs to two mesh approximation algorithms by measuring the Hausdorff distance (color scale from yellow to black) to the input mesh. The complexity of the LOD2, QEM [Garland and Heckbert 1997] and VSA [Cohen-Steiner et al. 2004] models is identical (190 facets). LOD2 without plane regularization has a lower root mean square error (RMS) than LOD2 with planar regularization but is less abstracted and consumes more time to reconstruct. In terms of structure-awareness, thin components such as the church towers are correctly preserved in the different LODs, which is not the case for mesh approximation algorithms. In addition, QEM and VSA do not fill the holes contained in the input mesh (see front right facade).

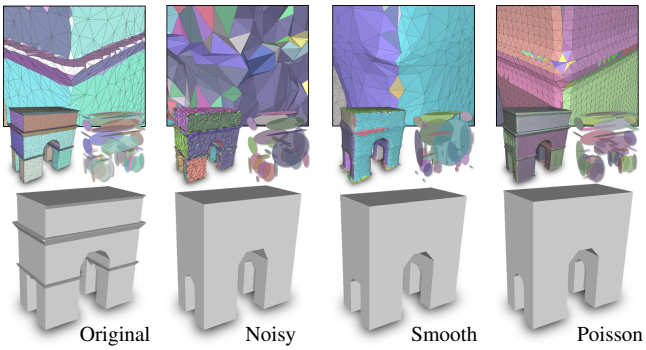

Fig. 18. Robustness. Left: "defect-free" input mesh colored by superfacets and its planar proxies (middle). Our reconstruction algorithm (applied here with no classification to evaluate only the proxy detection and abstraction steps) recovers most features (bottom). Notice the curved area reconstructed by planar polygons. Middle left: when noise is added the small scale features are filtered out and the vault is overly simplified. Right: when fed with the output of the Poisson reconstruction method the behavior of the algorithm is similar to the one on the smoothed mesh (middle right).

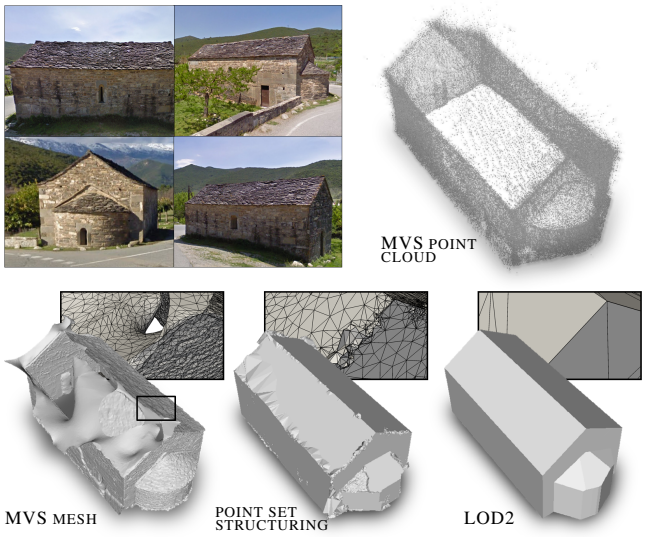

Fig. 19. Robustness to missing data. Reconstruction solely from ground-based images leads to major artifacts on roofs, leading to sparse point clouds, then meshes with holes and topological defects (left) using [Autodesk 2014]. Starting from such defect-laden mesh as input, our approach recovers the correct structure: the 3D planar arrangement yields high robustness due to the fact that each plane cuts the entire bounding box space without any spatial restriction. A direct structuring of the MVS point cloud [Lafarge and Alliez 2013] also fills some of the holes, but the noise and outliers strongly hampers the recovery of the sharp creases (see close-ups).

together with the semantic rules improve spatial consistency and reduce the number of classification errors. Fig.18 evaluates the robustness of the proxy detection and abstraction on an input mesh with variable scale features, noise and smoothed features. As shown by Fig.19, the pipeline is to some extend robust to missing data (small holes) in the input mesh. In particular, the arrangement of planes provides a means to reconstruct sharp creases and corners even when data are missing near the intersection of proxies. When holes are too large, the algorithm may fail detecting some planar proxies that are important to infer the correct structure.

Accuracy and abstraction. Fig.17 evaluates the accuracy of the reconstructed LODs against the input meshes, albeit our approach is designed to provide a tradeoff between faithfulness to input data and structure-aware abstraction. The comparisons against two mesh approximation approaches [Garland and Heckbert 1997; Cohen-Steiner et al. 2004], referred to as QEM and VSA respectively, show comparable approximation errors, better resilience to holes and topological artifacts of the input mesh through the arrangement of planes, and better coherence and preservation of thin structures across LODs such as the square church towers. Notice how LOD3 represents roof details such as chimneys and dormer-windows while keeping a low polygon count.

Input data. Deciding upon the best type of input data for urban reconstruction is a recurrent dilemma [Leberl et al. 2010]. While most existing approaches take point clouds as input, in particular LIDAR scans, we argue that dense meshes generated by MVS

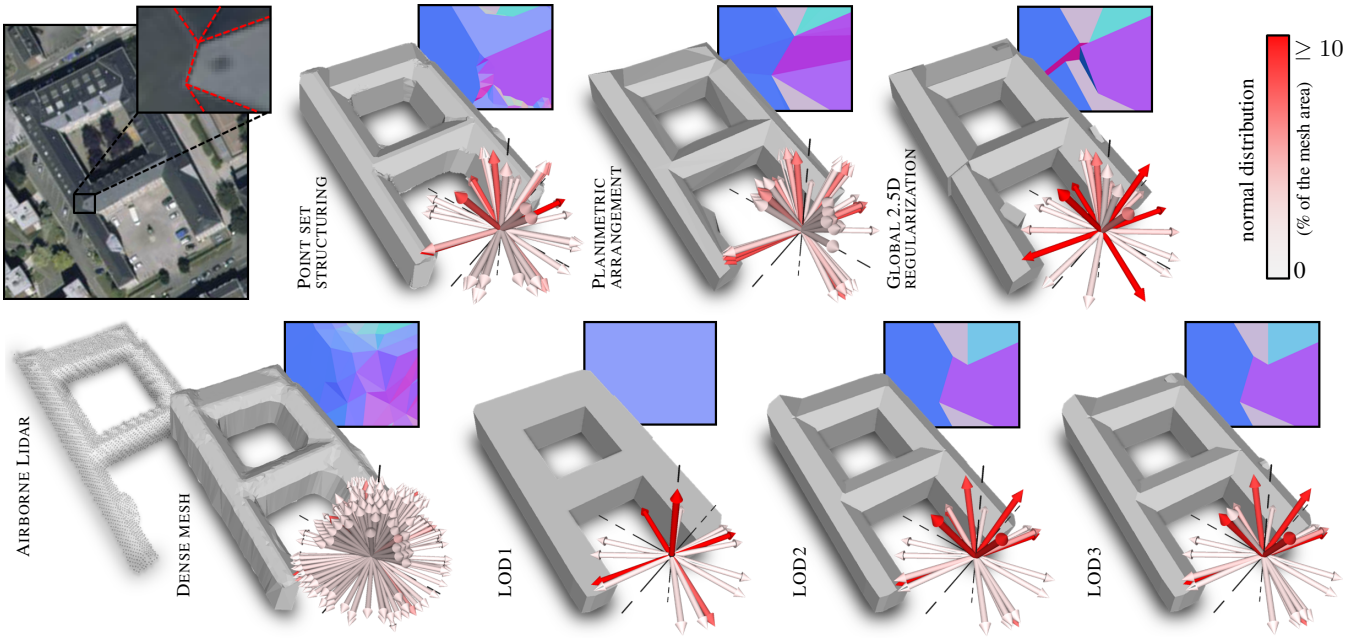

Fig. 20. Comparisons with urban reconstruction methods. Starting from a low-density airborne LIDAR point cloud, we generate a dense mesh using a standard elevation grid used as input to our algorithm. The two methods specialized to airborne LIDAR (planimetric arrangement [Lafarge and Mallet 2012] and global 2.5D regularization [Zhou and Neumann 2012]) as well as point set structuring [Lafarge and Alliez 2013] also provide low-complexity and structure-aware representations. However, our approach generates 3D models with higher level of abstraction through regularization, see the distribution of output normals where only one (resp. four) non-horizontal direction are required at LOD1 (resp. LOD2). As highlighted by close-ups (colored by normal directions), we recover non-trivial adjacency of roof sections with improved accuracy.

workflows offer significant advantages. Contrary to point clouds, MVS meshes have richer geometric and topological description derived from photo-consistency principles. To our knowledge, none of the existing surface reconstruction methods from point clouds are able to combine semantization and photo-consistency in order to generate abstracted LODs. Fig.20 describes a qualitative comparison of our approach against three specialized urban reconstruction methods from LIDAR scans based on planimetric arrangement [Lafarge and Mallet 2012], point set structuring [Lafarge and Alliez 2013], and global 2.5D regularization [Zhou and Neumann 2012].

Limitations. We limited the classification to four common classes of urban objects. At first glance such a low class number may appear restrictive in terms of semantics, but these four classes match CityGML and the requirements of several application needs. They provide a satisfactory tradeoff between robustness and quality of the reconstruction (We found only few errors during visual inspection of the large scale scene at LOD1 and LOD2 against the airborne tiled image, see Fig. 16). This choice hampers the reconstruction of less common urban structures such as bridges or elevated roads. Our 3-step pipeline is however amenable to inserting additional classes with new labels in the MRF-based classification, and new objects to abstract and reconstruct. The combination of large buildings and irregular non-flat ground can yield classification errors: e.g., sharp creases of the ground surface labeled as building, or large buildings labeled as ground. The use of planar proxies is also a limitation when dealing with freeform architecture buildings such as the dome of *Les Invalides* depicted by Fig.16.

At first glance our approach may be seen as a complex assembly: iconization on depth maps for trees, superstructures and facade elements, as well as 3D arrangements of primitives for buildings. A closer look however reveals that our methodological choices are specialized to the scale, structure and semantic of data. In addition, they are matching the limitations and constraints of real-world measurement data: despite recent advances on airborne acquisition the resolution of MVS meshes is too limited to handle roof superstructures with a process similar to the one applied on buildings. Methods specialized to high resolution depth maps reveal more appropriate for accurate faithful reconstruction of superstructures and facade elements.

7. CONCLUSIONS

Our work on LOD generation for urban scenes provides an automated framework to generate semantic-aware LODs from raw meshes. The four LODs generated are both meaningful and refineable thanks to a coherent design of the abstraction and reconstruction steps for the LODs (e.g., roof superstructures of LOD3 are reconstructed from height maps derived from the roofs computed in LOD2, and LOD0 is reconstructed by instantiating a 2D min-cut algorithm applied to a subset of abstracted proxies used in other LODs).

Our initial goal to devise a fully automated pipeline translates into a unsupervised classification method relying solely on geometric attributes and semantic rules. The classification is performing well with a small set of local geometric attributes and global solve. Our approach is shown to exhibit robustness to defect-laden meshes through regularized optimizations combined with 3D arrangements which generate well-behaved surfaces by construction. Our initial

goal to devise a scalable workflow is also met by exploiting both the classification and abstraction steps in order to instantiate one reconstruction process per building or per tree component, and to reduce the combinatorial complexity of the 3D arrangements.

As future work we wish to devise a photo-consistent framework by exploiting in all steps of our approach the color attributes of the multi-view stereo images. We will also investigate the fusion of airborne and ground-based measurements in order to reconstruct facade elements such as doors or windows with more details.

Acknowledgments

We wish to thank Acute3D, Autodesk, Interatlas, French mapping agency, Qian-Yi Zhou and Henrik Zimmer for providing datasets and materials for comparisons. This work is supported by an ERC Starting Grant "Robust Geometry Processing" (257474).

REFERENCES

ACUTE3D. 2014. http://www.acute3d.com/.

AREFI, H., ENGELS, J., HAHN, M., AND MAYER, H. 2008. Levels of Detail in 3D Building Reconstruction from LIDAR Data. In *Proc. of ISPRS conference*.

ARIKAN, M., SCHWARZLER, M., FLORY, S., WIMMER, M., AND MAIERHOFER, S. 2013. O-snap: Optimization-based snapping for modeling architecture. *ACM Transactions on Graphics 32,* 1.

ATTENE, M., KATZ, S., MORTARA, M., PATANE, G., SPAGNUOLO, M., AND TAL, A. 2006. Mesh segmentation - a comparative study. In *Proc. of Shape Modeling International*.

AUTODESK. 2014. http://www.123dapp.com/catch.

BAO, F., YAN, D.-M., MITRA, N., AND WONKA, P. 2013. Generating and exploring good building layouts. *ACM Transactions on Graphics*. Proc. of SIGGRAPH.

BOYKOV, Y. AND KOLMOGOROV, V. 2004. An experimental comparison of min-cut/max-flow algorithms for energy minimization in vision. *IEEE trans. on Pattern Analysis and Machine Intelligence 26,* 9.

BOYKOV, Y., VEKSLER, O., AND ZABIH, R. 2001. Fast approximate energy minimization via graph cuts. *IEEE trans. on Pattern Analysis and Machine Intelligence 23,* 11.

CHAUVE, A.-L., LABATUT, P., AND PONS, J.-P. 2010. Robust piecewise-planar 3D reconstruction and completion from large-scale unstructured point data. In *IEEE Conference on Computer Vision and Pattern Recognition*.

CHEN, X., GOLOVINSKIY, A., AND FUNKHOUSER, T. 2009. A Benchmark for 3D Mesh Segmentation. *ACM Transactions on Graphics*. Proc. of SIGGRAPH.

COHEN-STEINER, D., ALLIEZ, P., AND DESBRUN, M. 2004. Variational shape approximation. In *Proc. of SIGGRAPH Conference*. ACM.

COHEN-STEINER, D. AND MORVAN, J.-M. 2003. Restricted delaunay triangulations and normal cycle. In *Proc. of ACM Conference on Computational Geometry*.

COUGHLAN, J. M. AND YUILLE, A. L. 2000. The Manhattan world assumption: Regularities in scene statistics which enable Bayesian inference. In *Proc. of Neural Information Processing Systems*.

FALCIDIENO, B. AND SPAGNUOLO, M. 1998. A Shape Abstraction Paradigm for Modeling Geometry and Semantics. In *Proc. of the Conference on Computer Graphics International*.

FRUEH, C. AND ZAKHOR, A. 2003. Constructing 3D City Models by Merging Ground-Based and Airborne Views. In *IEEE Conference on Computer Vision and Pattern Recognition*.

FURUKAWA, Y., CURLESS, B., SEITZ, S., AND SZELISKI, R. 2009. Manhattan-world stereo. In *IEEE Conference on Computer Vision and Pattern Recognition*.

GARLAND, M. AND HECKBERT, P. 1997. Surface simplification using quadric error metrics. In *ACM SIGGRAPH Conference*.

GROGER, G. AND PLUMER, L. 2012. Citygml interoperable semantic 3d city models. *Journal of Photogrammetry and Remote Sensing 71*.

HAENE, C., ZACH, C., COHEN, A., ANGST, R., AND POLLEFEYS, M. 2013. Joint 3D scene reconstruction and class segmentation. In *IEEE Conference on Computer Vision and Pattern Recognition*.

JU, T. 2004. Robust repair of polygonal models. In *Proc. of SIGGRAPH Conference*. ACM.

KALOGERAKIS, E., HERTZMANN, A., AND SINGH, K. 2010. Learning 3d mesh segmentation and labeling. *ACM Transactions on Graphics*. Proc. of SIGGRAPH.

LAFARGE, F. AND ALLIEZ, P. 2013. Surface reconstruction through point set structuring. *Computer Graphics Forum 32,* 2. Proc. of EUROGRAPHICS.

LAFARGE, F., DESCOMBES, X., ZERUBIA, J., AND PIERROT-DESEILLIGNY, M. 2010. Structural approach for building reconstruction from a single DSM. *IEEE trans. on Pattern Analysis and Machine Intelligence 32,* 1.

LAFARGE, F. AND MALLET, C. 2012. Creating large-scale city models from 3D-point clouds: a robust approach with hybrid representation. *International Journal of Computer Vision 99,* 1.

LEBERL, F., IRSCHARA, A., POCK, T., MEIXNER, P., GRUBER, M., SCHOLZ, S., AND WIECHERT, A. 2010. Point clouds: Lidar versus 3d vision. *Photogrammetric Engineering and Remote Sensing 76,* 10.

LI, S. Z. 2001. *Markov Random Field modeling in Image Analysis*. Springer.

LI, Y., WU, X., CHRYSATHOU, Y., SHARF, A., COHEN-OR, D., AND MITRA, N. J. 2011. Globfit: Consistently fitting primitives by discovering global relations. *ACM Transactions on Graphics*. Proc. of SIGGRAPH.

LIN, H., GAO, J., ZHOU, Y., LU, G., YE, M., ZHANG, C., LIU, L., AND YANG, R. 2013. Semantic decomposition and reconstruction of residential scenes from lidar data. *ACM Transactions on Graphics*. Proc. of SIGGRAPH.

LUEBKE, D., WATSON, B., COHEN, J. D., REDDY, M., AND VARSHNEY, A. 2002. *Level of Detail for 3D Graphics*. Morgan Kaufmann Editions.

MARTINOVIC, A., MATHIAS, M., WEISSENBERG, J., AND VAN GOOL, L. 2012. A three-layered approach to facade parsing. In *European Conference on Computer Vision*.

MEHRA, R., ZHOU, Q., LONG, J., SHEFFER, A., GOOCH, A., AND MITRA, N. 2009. Abstraction of Man-Made Shapes. *ACM Transactions on Graphics*. Proc. of SIGGRAPH.

MITRA, N., WAND, M., ZHANG, H., COHEN-OR, D., AND BOKELOH, M. 2013. Structure-aware shape processing. In *EUROGRAPHICS State-of-the-art Report*.

MUSIALSKI, P., WONKA, P., ALIAGA, D., WIMMER, M., VAN GOOL, L., AND PURGATHOFER, W. 2013. A survey of urban reconstruction. *Computer Graphics Forum 32,* 6.

OESAU, S., LAFARGE, F., AND ALLIEZ, P. 2014. Indoor scene reconstruction using feature sensitive primitive extraction and graph-cut. *ISPRS Journal of Photogrammetry and Remote Sensing 90*.

PAULY, M., GROSS, M. H., AND KOBBELT, L. 2002. Efficient simplification of point-sampled surfaces. In *Visualization*. IEEE.

PIX4D. 2014. http://pix4d.com/.

POULLIS, C. AND YOU, S. 2009. Automatic reconstruction of cities from remote sensor data. In *IEEE Conference on Computer Vision and Pattern Recognition*.

RIEMENSCHNEIDER, H., KRISPEL, U., THALLER, W., DONOSER, M., HAVEMANN, S., FELLNER, D., AND BISCHOF, H. 2012. Irregular lattices for complex shape grammar facade parsing. In *IEEE Conference on Computer Vision and Pattern Recognition*.

ROTTENSTEINER, F., SOHN, G., JUNG, J., GERKE, M., BAILLARD, C., BENITEZ, S., AND BREITKOPF, U. 2012. The ISPRS benchmark on urban object classification and 3d building reconstruction. In *Proc. of the ISPRS congress*.

SHAMIR, A. 2008. A survey on mesh segmentation techniques. *Computer Graphics Forum 27,* 6.

SINHA, S., STEEDLY, D., SZELISKI, R., AGRAWALA, M., AND POLLEFEYS, M. 2008. Interactive 3d architectural modeling from unordered photo collections. *ACM Transactions on Graphics*. Proc. of SIGGRAPH Asia.

TEBOUL, O., SIMON, L., KOUTSOURAKIS, P., AND PARAGIOS, N. 2010. Segmentation of building facades using procedural shape prior. In *IEEE Conference on Computer Vision and Pattern Recognition*.

TOSHEV, A., MORDOHAI, P., AND TASKAR, B. 2010. Detecting and parsing architecture at city scale from range data. In *IEEE Conference on Computer Vision and Pattern Recognition*.

VANEGAS, C., ALIAGA, D., AND BENES, B. 2010. Building reconstruction using Manhattan-world grammars. In *IEEE Conference on Computer Vision and Pattern Recognition*.

VANEGAS, C., ALIAGA, D., AND BENES, B. 2012. Automatic extraction of manhattan-world building masses from 3d laser range scans. *IEEE Trans. on Visualization and Computer Graphics 18,* 10.

VANEGAS, C., ALIAGA, D., WONKA, P., MULLER, P., WADDELL, P., AND WATSON, B. 2010. Modeling the appearance and behavior of urban spaces. In *EUROGRAPHICS State-of-the-art Report*.

VERDIE, Y. AND LAFARGE, F. 2014. Detecting parametric objects in large scenes by monte carlo sampling. *International Journal of Computer Vision 106,* 1.

YUMER, M. E. AND KARA, L. B. 2012. Co-abstraction of shape collections. *ACM Transactions on Graphics*. Proc. of SIGGRAPH Asia.

ZEBEDIN, L., BAUER, J., KARNER, K., AND BISCHOF, H. 2008. Fusion of feature- and area-based information for urban buildings modeling from aerial imagery. In *European Conference on Computer Vision*.

ZHOU, K., ZHANG, E., BITTNER, J., AND WONKA, P. 2008. Visibility-driven mesh analysis and visualization through graph cuts. *IEEE Trans. on Visualization and Computer Graphics 14,* 6.

ZHOU, Q. AND NEUMANN, U. 2012. 2.5D building modeling by discovering global regularities. In *IEEE Conference on Computer Vision and Pattern Recognition*.